ELSEVIER

Polymer 43 (2002) 4251–4260

polymer

www.elsevier.com/locate/polymer

Comparison of solution intercalation and melt intercalation of polymer–clay nanocomposites

Zhiqi Shen[a], George P. Simon[b,*], Yi-Bing Cheng[b]

[a]*DBCE, CSIRO, P.O. Box 56, Highett, Vic. 3190, Australia*
[b]*School of Physics and Materials Engineering, Monash University, P.O. Box 69M, Clayton, Vic. 3800, Australia*

Received 24 January 2002; received in revised form 18 March 2002; accepted 21 March 2002

Abstract

Polymer–clay nanocomposites of poly(ethylene oxide)/Na-montmorillonite (PEO/MMT) and PEO/organo-modified bentonite (B34) systems prepared via solution intercalation and melt intercalation have been compared by X-ray diffraction and Fourier transform infrared (FTIR) analysis. The gallery size of solution-intercalated hybrids in both PEO/MMT and PEO/B34 systems increases with PEO content up to a plateau level at 15%. However, the gallery size of melt-intercalated PEO/MMT and PEO/B34 hybrid remains the same regardless of the PEO concentration. FTIR analysis shows no difference in spectrum of samples prepared by solution intercalation compared to melt intercalation. The PEO conformation in the PEO/clay intercalated hybrids is concluded to be a distorted helical structure.

Keywords: Polymer–clay nanocomposites; Melt intercalation; Solution intercalation

1. Introduction

Intercalation of polymers in layered hosts, such as mica type silicates has proven to be a successful approach to synthesize nanophase organic–inorganic hybrids. The preparative methods are divided into three groups according to starting materials and processing techniques: in situ polymerization intercalation, solution intercalation and melt intercalation. Polymerization intercalation is a method based on the use of one or more monomers that may be in situ linearly polymerized or crosslinked and was the first method used to synthesize polymer–layered silicate nanocomposites based on polyamide 6 [1,2]. It is still widely used in many studies, especially in thermosetting polymer–layered silicate nanocomposites. However, it is not relevant to the work presented in this paper, and will not be discussed further. Polymer solution intercalation is based on a solvent system in which the polymer is soluble and the silicate layers are swellable [3]. The layered silicate is first swollen in a solvent, such as water, toluene or chloroform. When the polymer and silicate solutions are mixed, the polymer chains intercalate and displace the solvent within the interlayer of the silicate. Upon solvent removal, the intercalated structure remains, resulting in hybrids with nanoscale morphology. Water soluble polymers, such as polyvinyl alcohol [3], poly(vinyl pyrrolidinone) [4], poly(ethylene oxide) (PEO) [5,6] and poly(ethylene vinyl alcohol) [7] have been intercalated into clay galleries via this method. Examples including non-aqueous solvents are of nanocomposites of a poly(1-lactide)–clay system [8] or PEO [9] in chloroform as a cosolvent, and polyimide–aluminum nitride system in *N*-methylprolidinone as the suspension media [10] and high-density polyethylene with xylene and benzonitrile [11]. Nematic liquid crystal polymer–clay nanocomposites have also been prepared in various organic solvents, such as toluene and DMF [12].

The thermodynamics involved in solution intercalation are as follows. For the overall process, in which polymer is exchanged with the intercalated solvent in the gallery, a negative variation in the Gibbs free energy is required. The driving force for polymer intercalation into layered silicate from solution is the entropy gained by desorption of solvent molecules, which compensates for the entropy decrease of the confined, intercalated chains [13]. Intercalation only occurs for certain polymer/solvent pairs via solution intercalation. It is a good way to intercalate polymers with little or no polarity into layered structures, and facilitates production of thin films with polymer, oriented-clay intercalated layers. However, in a commercial sense, it involves the use

* Corresponding author.
E-mail addresses: shirley.shen@csiro.au (Z. Shen), george.simon@spme.monash.edu.au (G.P. Simon), yibing.cheng@spme.monash.edu.au (Y.-B. Cheng).

0032-3861/02/$ - see front matter
PII: S0032-3861(02)00230-6

of large amount of organic solvents, which is usually environmentally unfriendly and economically prohibitive.

Melt intercalation is becoming attractive since it came to prominence in 1990s [14]. Quite a number of polymers, such as PEO [15,16], polystyrene and a series of styrene-derivative polymers [14,17,18], poly(styrene-*b*-butadiene) copolymer [19], polyamide 6 [20] and polyethylene–poly(ethylene glycol) diblock copolymer [21] have been melt intercalated into clays, predominantly into layered silicates that have been organo-modified. The melt intercalation method has great advantages over either polymerization intercalation or polymer solution intercalation. Firstly, this method is environmentally benign due to the absence of organic solvents. Secondly, it is compatible with current industrial mixing and processing techniques. Nanocomposites can, therefore, be manufactured using industrial processes, such as extrusion and injection molding [22,23]. The melt intercalation method allows the use of polymers which were previously not suitable for polymerization or solution intercalation. The effects of processing parameters, such as annealing temperature and time and pressure applied to green body on melt intercalation of PEO/sodium montmorillonite (MMT) and PEO/organo-modified bentonite (B34) systems have been previously reported [24].

It is rare that solution intercalation has been studied alongside melt intercalation in the same polymer–silicate system. In this paper, the results of solution intercalation are compared with those of melt intercalation of PEO into an untreated MMT or a B34 clays. These two materials were chosen because of their wide availability and high usage, having been reported in a number of nanocomposite studies. This should allow further understanding of the structure of intercalated hybrids by comparing the similarities and differences between the intercalated hybrids made by these two methods. A possible structural model of PEO/MMT hybrid (particular for the conformation of PEO chains in hybrid gallery) is also proposed based on these comparisons.

2. Materials and methods

The polymer used in this work was PEO, of average $M_n = 172\,700$ and PD = 2.58, and was obtained from Aldrich Chemical Company, Inc. The molecular weights of PEO were determined in DMF at 25 °C on a Viskotek Triple Detector GPC (Shimadzu Chromatograph and Viskotek T60A Dual Detector) using a PEO standard of $M_n = 217\,800$ and PD = 1.02.

MMT used was obtained from University of Missouri, Columbia, Source Clay Minerals Repository in USA and has a cation exchange capacity (CEC) of 80 mequiv./100 g and used as received and after being heated at 250 °C for 200 min to allow for removal of molecular water in the galleries. B34, which is a cation-exchanged bentonite, was obtained from Rheox (USA) with no CEC given and used as received. The galleries of B34 are occupied by organo-modified cations, dimethylditallow ammonium cations. The formula of dimethylditallow ammonium cations is $(CH_3)_2N^+(CH_3(CH_2)_{13,15,17})_2$ with $C_{14} \sim 5\%$, $C_{16} \sim 25\%$, and $C_{18} \sim 70\%$. The organic content in the B34 is about 31 wt% and the upper used temperature of B34 for melt intercalation is thus around 220 °C according to thermogravitic analysis.

Table 1
Summary of the results of solution intercalation

Silicate	Ratio of PEO to silicate	Solvent	Intercalation
Na-MMT	5:95–40:60	Water	Full intercalation
B34	15:85	Toluene	Very little
B34	15:85, 30:70	Chloroform	Full intercalation

For solution intercalation, the selected polymer and silicate were weighed according to the designated ratio, and the polymer dissolved into an excess amount of a suitable solvent, the silicate added to the solution and stirred for 1 day. The solvents used for attempted solution intercalation were water, toluene and chloroform. The solvent was removed by placing the container in a vacuum oven at a suitable temperature (no greater than 50 °C), the resultant material stored in a desiccator. Table 1 summarizes the solution intercalation in terms of polymers, layered silicates and the polymer weight percentages, solvents used and the success or otherwise of the attempted solution intercalation. The success of intercalation is mainly verified by the increase of the (001) *d*-spacing, determined by X-ray diffraction (XRD) analysis. Selection of an appropriate solvent plays a very important role in solution intercalation. High solubility of polymer and good dispersion of silicate are the primary criteria used in the solvent selection of good solution intercalation. For example, PEO does not intercalate well into B34 from toluene, but does from chloroform. Toluene likewise is a non-polar solvent, and does not readily dissolve PEO and thus PEO cannot intercalate well into silicates from toluene.

Melt intercalation was undertaken as follows. Powders of polymer and silicate with the required weight ratios of polymer-to-silicate were mechanically mixed using an agate mortar and pestle and formed into pellets using a hydraulic press at 70 MPa. Polymer melt intercalation was accomplished by annealing the pressed pellets in an electrical resistance furnace at either 85 or 95 °C and the annealing time allowed for full intercalation to take place was about 8 h. Compositions of the mixtures in either solution or melt intercalation are all represented as weight percent of polymer in the paper.

XRD patterns were collected on a Rigaku-Geigerflex X-ray diffractometer using Ni filtered Cu Kα radiation. The scanning speed was 1 °/min, and the step 0.05°. When an internal reference (silicon powder) was used, the specimens were made by adding 10 wt% of silicon powder into

sample powder. Powders were either loosely packed in horizontally held trays or spread out on glass slides.

Fourier transform infrared (FTIR) spectra of samples were collected on a Perkin Elmer 1600 FTIR from 400 to 4000 cm^{-1} with a nominal resolution of 2 cm^{-1}. For each spectrum, 64 runs were collected and averaged. The specimens were made by adding ~1 wt% of the sample powder to dry KBr powder and pressed into a disc of 13 mm in diameter and 1–2 mm thick under vacuum.

3. Results and discussion

3.1. Comparison of XRD results of the PEO/MMT system

XRD patterns supply very useful information of the gallery size of the final intercalated hybrids by measuring the increase of basal (001) *d*-spacing [14,15,25]. Fig. 1 shows the XRD patterns of the hybrid samples with different PEO contents via melt or solution intercalation. The melt intercalation of the PEO/MMT system with different polymer/silicate ratios has been discussed previously [24]. The *d*-spacing of the (001) peak shifts directly from 9.6 Å ($2\theta = 9.23°$) in the dry MMT to 17.9 Å ($2\theta = 4.95°$) in the intercalated hybrid after annealing at 85 °C for 8 h. No intermediate step of the (001) *d*-spacing occurs in the melt-intercalated sample, even for very low PEO contents. Fig. 1(a) and (b) only shows an example for PEO/MMT hybrid obtained via melt intercalation at PEO concentration of 5 and 25%, respectively. The (001) peak of dry MMT at $2\theta = 9.23°$ ($d = 9.6$ Å) can be seen in Fig. 1(a), as well as the (001) peak of the hybrid at $2\theta = 4.95°$ ($d = 17.9$ Å). This means the pristine MMT also remains in the final material, in addition to the PEO/MMT intercalated hybrid when PEO content is only 2%.

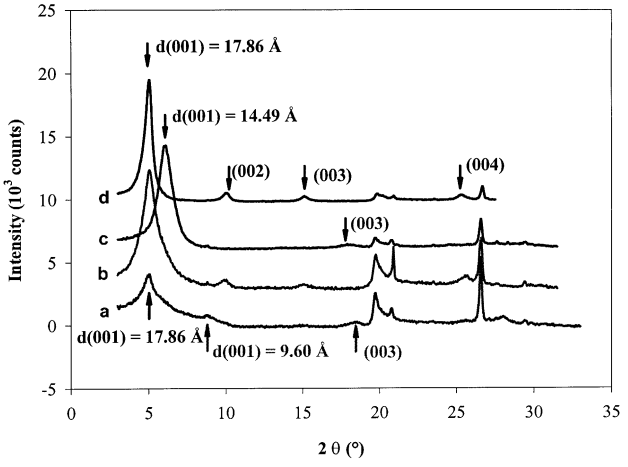

Fig. 1. XRD patterns of the samples with different PEO/MMT ratios via melt intercalation (annealing at 95 °C for 8 h) and solution intercalation (in water). (a) 5% PEO in PEO/dry MMT system after melt intercalation, (b) 25% PEO in PEO/dry MMT system after melt intercalation, (c) 5% PEO in PEO/MMT system after solution intercalation, and (d) 20% PEO in PEO/MMT system after solution intercalation.

The hybrid obtained via solution intercalation does, however, increase its gallery size as a function of increasing PEO content. The (001) peak of the PEO/MMT hybrid with 5% PEO obtained via solution intercalation is at $d = 14.5$ Å ($2\theta = 6.10°$), seen in Fig. 1(c), which is between $d = 17.9$ Å for a fully intercalated hybrid and $d = 9.6$ Å for dry MMT. The gallery size in this sample is 4.9 Å after solution intercalation. The XRD pattern of this sample with 5% PEO via solution intercalation is quite different from that with the same PEO content for melt intercalation. However, the (001) peak of the PEO/MMT hybrid with 25% PEO obtained via solution intercalation is at $d = 17.9$ Å ($2\theta = 4.95°$), shown in Fig. 1(d), and is at the same position as that of the hybrid with the same PEO concentration (25%) obtained via melt intercalation. The gallery size of the PEO/MMT hybrids is thus the same, 8.3 Å, for concentration of 25% PEO using both methods.

Fig. 2 shows more XRD patterns of samples with various PEO/MMT ratios via solution intercalation. There is clearly a dominant peak of (001) at $d = 14.9$ Å in each pattern of both samples of 10% PEO (Fig. 2(b)) and 12.5% PEO (Fig. 2(c)), and a shoulder in the (001) peak is also observed at approximately $d = 16.7$ and 17.0 Å, for the different concentrations.

In particular, the series of the (00*l*) peaks (except (001)) of the sample of 12.5% PEO occur at the same positions as those in a sample for PEO contents greater than 15%, as seen for the (002) peak in Fig. 2. Note that a weak shoulder peak at about $d = 14.5$ Å appears when the dominant peak is at $d = 17.9$ Å in the XRD pattern of the sample of 15% PEO (Fig. 2(d)). The broad peak between 17.0 and 14.9 Å in both samples in Fig. 2(b) and (c), respectively, may be explained by the existence of clays with a range of spacings. Note that the half height width of (001) peak in the sample of 5% PEO is much greater than that of 15–25% PEO. This suggests that the gallery sizes (reflected by the (001) peak)

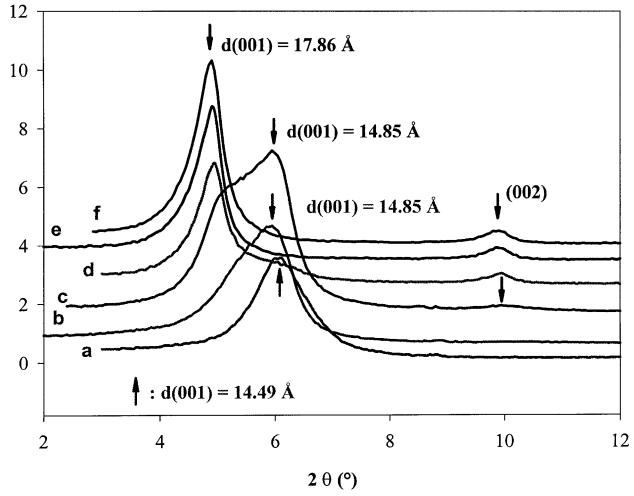

Fig. 2. XRD patterns of the PEO/MMT hybrids with various polymer contents via solution intercalation (in water). (a) 5% PEO, (b) 10% PEO, (c) 12.5% PEO, (d) 15% PEO, (e) 20% PEO, and (f) 25% PEO.

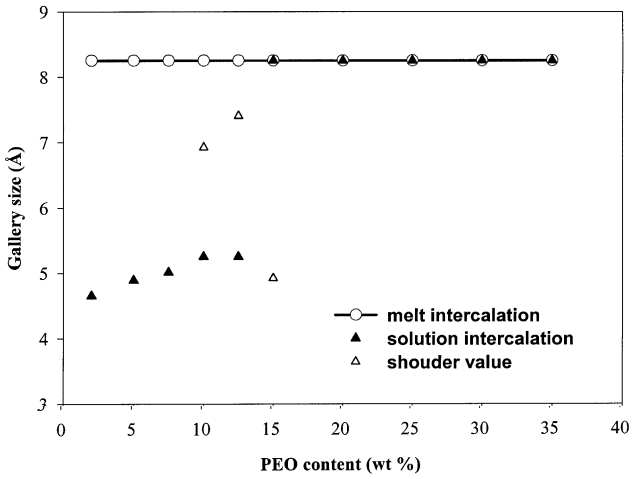

Fig. 3. Gallery size of PEO/MMT hybrid from both melt and solution intercalation as a function of PEO content in physical mixture before intercalation.

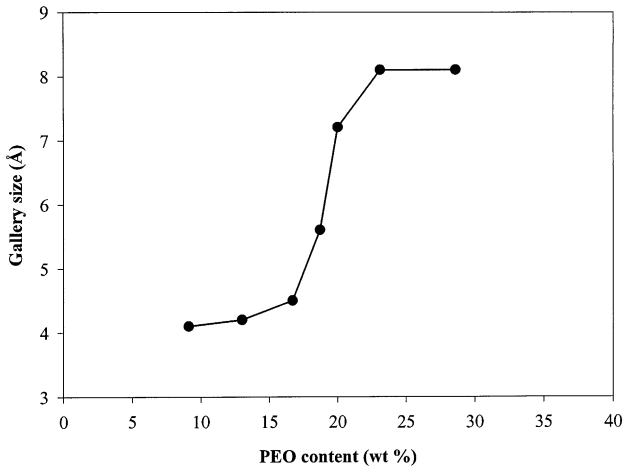

Fig. 4. Redrawn data of gallery size vs. PEO content converted from a figure of (001) *d*-spacing vs. PEO/MMT ratio from their paper [26] (the scale remains the same as in Fig. 3 to allow comparison).

in the sample with low PEO content are not as uniform as those are in the sample with higher PEO content, with different clay galleries being filled by differing amounts of PEO.

Fig. 3 shows the gallery size of the PEO/MMT hybrid (deduced from the XRD result) as a function of PEO content via melt and solution intercalation. It is clear that the gallery size of the PEO/MMT hybrid via solution intercalation increases gradually with PEO content up to PEO contents of 15%, after which it rapidly increases to 8.3 Å. It subsequently remains constant for further PEO additions. When the PEO content is less than 15%, the main gallery size (illustrated by the solid triangles) is about 4.7–5.3 Å, although in some samples a gallery size determined from the location of the shoulder peak on the main (001) peak can be seen and is shown as unfilled triangles. The unfilled circles show the gallery size (8.3 Å) for all samples with various PEO contents for the hybrids produced via melt intercalation, constant even for low concentrations.

Wu and Lerner [26] reported a similar result with a slightly different gallery size and a different boundary polymer/silicate ratio when they studied PEO/Na-MMT nanocomposites via solution intercalation using acetonitrile (CH_3CN) or water as a solvent. The molecular weight of PEO they used was from Aldrich of 100 K [26]. Since they used a different expression for the weight ratios of polymer to silicate, their concentrations of PEO have been converted to values consistent with presentation of the other data in this work. The range of PEO contents in their study was between 9.1 and 28.6%, and the gallery size of samples, in which contents of PEO up to 16.7% were used, was about 4 Å. They also found two intermediate (001) *d*-spacings of the hybrids between 16.7% PEO and 23.1% PEO. Fig. 4 shows gallery size vs. PEO content converted from the data for the PEO/MMT ratios (g/g) in their paper [26].

The basic *d*-spacing of (001) of the pristine MMT in their work was also 9.6 Å. The gallery size was 8.1 Å for high PEO contents and ~4 Å for lower PEO contents. As for the result presented here, the gallery size is 8.3 Å for high PEO contents and around 4.7–5.3 Å for low PEO concentrations. A significant difference between the previous report and this study is the PEO content in which the gallery size increases from small to greater values. The gallery size was still ~4 Å when PEO content was 16.7%, increasing to ~8 Å for greater concentrations (Fig. 4). In our work, the gallery already reaches 8.3 Å for PEO contents of 15%, shown in Figs. 2 and 3. Only a shoulder occurs in the patterns for samples of our work, although these have intermediate PEO contents, the intermediate (001) peaks were not observed. However Wu and Lerner [26] found two intermediate (001) values shown in Fig. 4, and they claimed that the two phases were single and double layers of PEO conformation within the MMT gallery.

3.2. Comparison of XRD results of the PEO/B34 system

Solution intercalation of the PEO into B34 was also attempted using toluene or chloroform for various PEO concentrations (note, in the PEO/B34 system, the polymer saturation ratio was determined to be 15:85 via melt intercalation [25]). PEO was able to intercalate into B34 via solution intercalation in chloroform, as shown in Fig. 5(a). Fig. 5(b) shows the XRD patterns of PEO/B34 hybrids of 15% PEO via melt intercalation as a comparison. The values of the (001) *d*-spacing of the samples of 15% PEO via solution intercalation are 36.8 Å, the same as that of samples produced via melt intercalation.

Fig. 6 shows the XRD result for the PEO/B34 hybrid obtained via solution intercalation in toluene and melt intercalation, compared to the spectrum for B34 itself. The (001) *d*-spacing of the PEO/B34 hybrid (15% PEO) obtained in toluene via solution intercalation is 33.2 Å, whilst that obtained via melt intercalation is 36.8 Å with the same

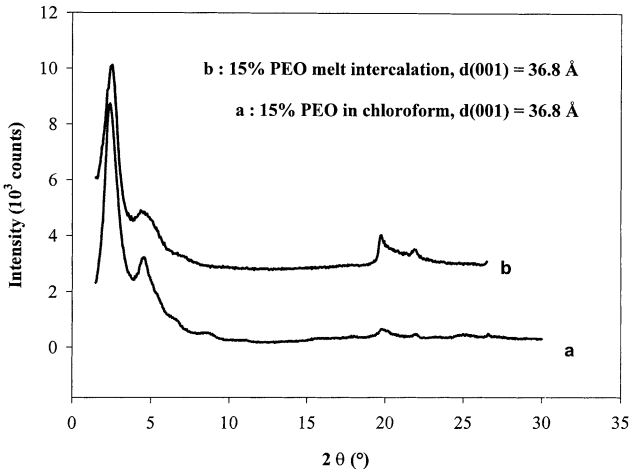

Fig. 5. XRD patterns for the PEO/B34 systems. (a) 15% PEO via solution intercalation in chloroform, and (b) 15% PEO via melt intercalation.

amount of PEO (15%) in the mixture samples. The XRD pattern of the final hybrid produced via melt intercalation (Fig. 6(c)) does not show any peak at the original peak positions of crystalline PEO. However, the XRD pattern of the final hybrid via solution intercalation (Fig. 6(b)) show broad peaks around the original positions of crystalline PEO peaks, suggesting that not all PEO has entered the hybrid gallery. In addition, the (002) peak of the hybrid obtained via solution intercalation in toluene (Fig. 6(b)) is not as well developed as that obtained via melt intercalation (Fig. 6(c)), further evidence that PEO does not fully intercalate into the B34s gallery via solution intercalation in toluene. The gallery size of melt-intercalated PEO/B34 hybrid does not change with PEO content [24], as for PEO/MMT system obtained via melt intercalation.

In the sample of 15% PEO via solution intercalation in toluene, the gallery size is about 3.6 Å, which is some 53% of the fully developed gallery size (6.8 Å). This is comparable with the relative gallery size in PEO/MMT hybrid via solution intercalation. Table 2 summarizes the gallery size in both the PEO/MMT and PEO/B34 systems. G_1 is the gallery size measured in the hybrid produced via solution intercalation and G_2 is the gallery size obtained in the same hybrid but via melt intercalation. The PEO/B34 hybrid with 15% PEO produced via solution intercalation in toluene is very similar to that of the PEO/MMT hybrid with 2% PEO produced in water. This implies that only few percent of PEO can intercalate into MMT via toluene and it appears not to be a good solvent for solution intercalation of the PEO/B34 system.

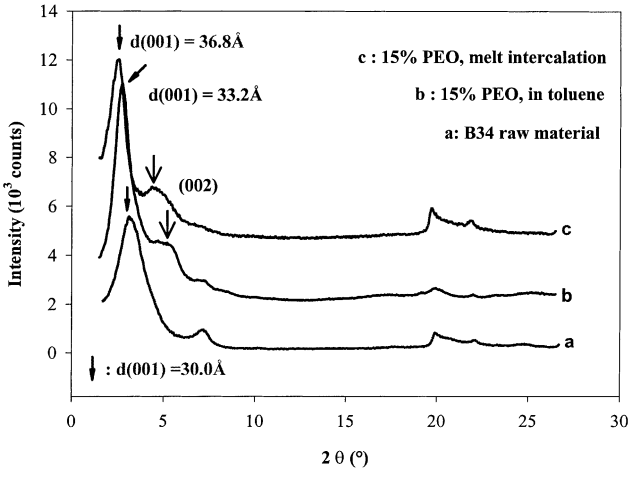

Fig. 6. XRD patterns for the PEO/B34 systems. (a) Pure B34, (b) 15% PEO via solution intercalation in toluene, and (c) 15% PEO via melt intercalation.

Table 2
Gallery size in the PEO/MMT and PEO/B34 hybrid via solution intercalation (G_1 is the gallery size in the hybrid produced via solution intercalation and G_2 is the gallery size obtained in the same hybrid via melt intercalation)

System (solvent)	G_1 (Å)	G_2 (Å)	G_1/G_2 (%)
PEO/MMT = 15:85 (in water)	8.3	8.3	100
PEO/MMT = 2.98 (in water)	4.7	8.3	56.6
PEO/B34 = 15:85 (in toluene)	3.6	6.8	53.0

In summary, the main finding is that in the PEO/B34 system, the gallery size increases with the PEO content via solution intercalation with PEO content, but does not show an increase via melt intercalation for a range of PEO concentrations. This behavior is also found in the PEO/MMT system, which implies that these two systems share a similar structural model in terms of polymer conformation in the clay gallery.

3.3. Comparison of FTIR results of the PEO/MMT system

Although XRD supplies information on the gallery size from the increase of basal spacing, the structure of the polymer itself cannot be deduced from XRD results due to the very low (if any) crystallinity of the polymer in the hybrid gallery. Spectroscopic techniques, such as IR, Raman and NMR are useful in order to establish the PEO structure inside the gallery, as well as the existence of interactions between the PEO chains and the cations in the gallery. A brief introduction to previous IR analyses on PEO, PEO–alkali metal salt complexes and PEO–clay nanocomposites is summarized prior to results being presented and discussed.

PEO has been studied extensively in last 40 years by IR or Raman spectroscopy. Vibrational studies have been carried out on the PEO in the crystalline state [27–30], in molten state [31,32], in aqueous solution [33,34] and in chloroform solution [33,34]. For the crystalline PEO, these conformational assignments have been supported by normal coordinate treatments of various skeletal models [34] and by detailed X-ray analysis [35]. PEO is found to have a helical structure in the crystalline state. The polymer chain has seven CH_2CH_2O units in two turns of the helix with a crystallographic repeat distance of 19.3 Å. The conformation

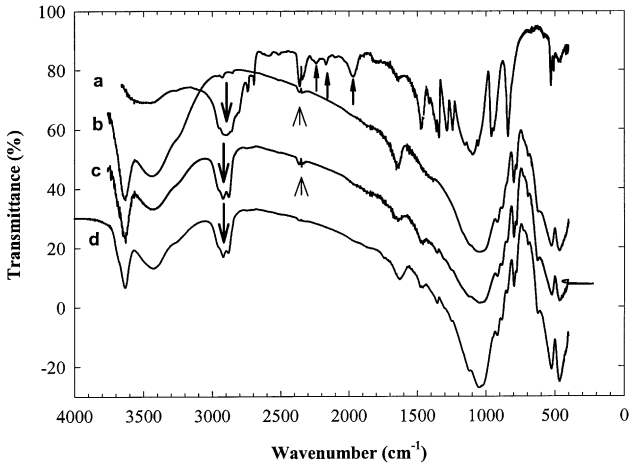

Fig. 7. FTIR spectra for the PEO/MMT system. (a) PEO, (b) dry MMT, (c) PEO/MMT hybrid via solution intercalation, and (d) PEO/dry MMT hybrid via melt intercalation (15% PEO in (c)).

along this chain are nearly *trans* (CC–OC), *trans* (CO–CC) and *gauche* (OC–CO). The CH_2 rocking modes found in the 1000–700 cm^{-1} region are particularly sensitive to conformational changes.

The vibrational spectroscopy and structure of a number of PEO complexes of alkali metal salts have also been studied [36]. In particular, NaX and KX complexes of PEO are believed to be in the crystalline state and have a helical configuration for the polymer, some of the PEO chains possibly wound around the alkali cations. The conformation may be approximated as a compressed helix, as opposed to the more extended and open helix of pure crystalline PEO.

The IR spectra of PEO/MMT nanocomposites have been recently studied [37–39]. The preparation method in those studies was solution intercalation using water or acetonitrile as a solvent. The ratio of PEO/MMT was not determined in those studies [37–39], but excess PEO (to the amount necessary to saturate the gallery) was likely since characteristic PEO peaks in the corresponding X-ray diffractograms could be seen, and could be removed by washing with acetonitrile followed by methanol. A helical structure of PEO in the gallery of the hybrid was claimed in those studies, supported by ^{23}Na NMR results and by comparing their IR results with those from PEO–alkali salt complexes [37–39].

However, the FTIR absorption bands in this study did not show precisely the same details as in the previous reports. Fig. 7 shows the FTIR spectra from 4000 to 400 cm^{-1} for PEO, dry MMT and PEO/MMT hybrids via either solution intercalation using water as the solvent or melt intercalation. Table 3 summarizes the frequency of all the absorption bands and the associated assignments. Note that a weak band at 778 cm^{-1}, which is due to the Si–O vibration of the quartz impurity in the MMT [40], is not included in the table. The double bands at 2360 and 2340 cm^{-1}, indicated by bigger upwards arrows, appeared in some samples and are due to gaseous CO_2 which originated from the air environment.

The most significant changes upon intercalation, indicated by the downward arrows in Fig. 7, correspond to the stretching and deformation vibration of the methylene groups. Pure PEO exhibits a large, broad band of asymmetric CH_2 stretching between 2940 and 2840 cm^{-1} and two narrow bands of lower intensity at 2740 and 2692 cm^{-1}. In the intercalated hybrids, these bands are transformed in two well-defined bands at 2918 and 2880 cm^{-1}, the changes having been reported previously [39]. In relation to the CH_2 stretching bands, which appear in the 1500–1200 cm^{-1} region, the most notable changes occur to the band at 1342 cm^{-1} which are shifted to 1360 cm^{-1} in the intercalated hybrids.

In a previous study [39], the original band at 1350 cm^{-1} was split into two bands at 1360 and 1342 cm^{-1} in the intercalated hybrid. This was interpreted in terms of ion–dipole interactions between the oxygen atoms of oxyethylene units, and the interlayer cations. It can, thus, be inferred that PEO interacts with the interlayer cations in a similar manner to conventional PEO–salt complexes.

Aranda and Ruiz-Hitzky [37,38] claimed that the spectra were indicative of the presence of *gauche* conformations of the $-CH_2-CH_2-$ groups, as required for a helical PEO conformation. The factors supporting this assignment were as follows: (i) the presence of two bands near 945 and 850 cm^{-1} assigned to CH_2 rocking vibrations of methylene groups in the *gauche* conformation, like in PEO–salt complexes [36] and (ii) the absence of a characteristic IR band near 1320 cm^{-1} assigned to CH_2 stretching vibration of ethylene groups in the *trans* conformation [36].

In this study, the two bands at 945 and 840 cm^{-1} which have been related to helical structures are only clearly observed in the pure PEO sample, and are not apparent in the intercalated hybrid. Note that the bands at 2240, 2170 and 1970 cm^{-1}, indicated by upward arrows in Fig. 7 in the spectrum of the pure PEO sample, are also not observed for the hybrids. To highlight this observation, detailed spectra between 1000 and 400 cm^{-1} in Fig. 7 are enlarged and shown in Fig. 8. The band at 945 cm^{-1} in pure PEO (illustrated by thinner upward arrows) is not observed in the hybrid, whilst the band at 840 cm^{-1} in pure PEO (thinner upward arrow) also disappears. Instead, a broad weak band centered at 846 cm^{-1} (thinner downward arrow), which may overlap with the band originally shown in pristine MMT at 848 cm^{-1} due to Al–O–H stretching in the silicate layers, can be seen. Though the characteristic band near 1320 cm^{-1} for CH_2 *trans* conformation (illustrated by short lines) is absent in all samples shown in Fig. 8, a new band at 1356 cm^{-1} (bigger upward arrow) appears in the hybrids. The two bands of CH_2 twisting vibration at 1282 and 1242 cm^{-1} in pure PEO shift to higher frequencies of 1300 and 1270 cm^{-1} and become weaker (bigger downward arrows). Since the IR absorption bands of samples are compared to that of crystalline PEO with a helical

Table 3
IR absorption bands and their assignments of PEO, dry MMT and PEO/MMT hybrid (4000–400 cm^{-1}) (mode assignments: ν (stretching); δ (bending); w (wagging); t (twisting); r (rocking). The subscripts a and s denote the asymmetric and symmetric motions with respect to the twofold axis perpendicular to the helix axis and passing through the O atom or through the center of the C–C bond)

Frequency (cm^{-1})	Frequency in reference (cm^{-1})	Assignment	Appearance in materials	Reference
3630	3624	ν(O–H)	MMT, hybrid	[42]
3440	3420	ν(O–H)	MMT, hybrid	[40]
2940–2840	2943	$\nu(CH_2)_a$	PEO	[43]
2940–2840	2887	$\nu(CH_2)_s$	PEO	[43]
2918	2923, 2910	$\nu(CH_2)_a$, $\nu(CH_2)_a$	Hybrid, hybrid	[43], [37]
2880	2883, 2878	$\nu(CH_2)_s$, $\nu(CH_2)_s$	Hybrid, hybrid	[43], [37]
2740	2741	$\nu(CH_2)$	PEO	[44]
2692	2696	$\nu(CH_2)$	PEO	[44]
2360	2347	CO_2 gaseous	Air atmosphere	[44]
2240	2240		PEO	[44]
2170	2172		PEO	[44]
1970	1968		PEO	[44]
1640	1662, 1630	ν(C–O), ν	PEO; MMT	[44]
1475	1473	$\delta(CH_2)_a$	PEO, hybrid	[36]
1462	1461	$\delta(CH_2)_a$	PEO, hybrid	[36]
1455	1453	$\delta(CH_2)_a$	PEO, hybrid	[36]
1362	1358	$w(CH_2)_s$	PEO	[36]
1356	1360	$\delta(CH_2)_a$	Hybrid	[37]
1342	1342	$w(CH_2)_a$	PEO	[36]
1282 → 13	1283	$t(CH_2)_a$	PEO, hybrid	[36]
1242 → 12	1244	$t(CH_2)_a$	PEO → hybrid	[36]
1150	1147	$\nu(COC)_a$	PEO → hybrid	[36]
1120	1115	ν(Si–O)	MMT, hybrid	[40]
~ 1100	~ 1103	$\nu(COC)_a$	PEO, hybrid	[36]
1040	1040	ν(Si–O)	MMT, hybrid	[45]
962	958	$r(CH_2)_a$	PEO	[36]
945	948	$r(CH_2)_s$	PEO	[36]
840	844	$r(CH_2)_s$	PEO	[36]
916, 880	915, 878	ν(Al–O–H)	MMT, hybrid	[40]
840, 800	845–835, 796	ν(Al(Mg)–O–	MMT, hybrid	[40]
525, 470	522, 467	ν(Al(Mg)–O–Si)	MMT, hybrid	[40]

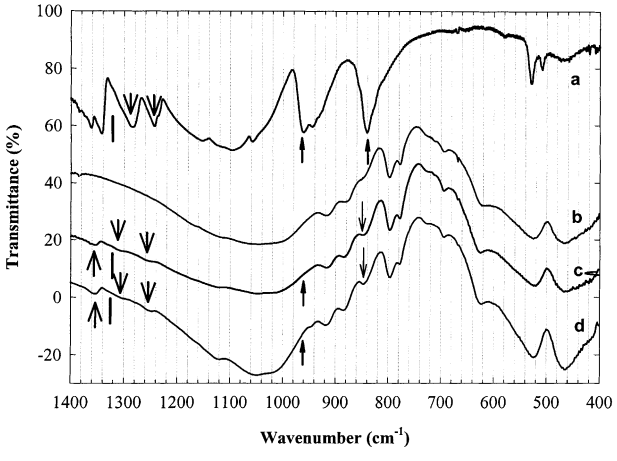

Fig. 8. FTIR spectra between 1400 and 400 cm^{-1} of the same samples as in Fig. 7. (a) PEO, (b) dry MMT, (c) PEO/MMT hybrid via solution intercalation, and (d) PEO/dry MMT hybrid via melt intercalation (25% PEO in (c)).

conformation, it leads to the conclusion that the PEO helical conformation is highly distorted, or at least rather stretched, if indeed it still exists.

The other main finding for the comparison of melt to solution intercalation is that no significant difference is observed in their FTIR spectra of final hybrids with 25% PEO prepared by these two methods (shown in Figs. 7 and 8). Indeed, there is no significant difference in IR spectra between these two preparation methods for various PEO contents, other than 25% PEO as well.

The broad band centered at 846 cm^{-1} in the sample of 25% PEO (illustrated by thinner downward arrows in Fig. 8) seems to shift to slightly lower frequencies with decreasing PEO content. The band center is at 842, 844, 844 and 846 cm^{-1}, when the PEO content is 5, 10, 15 and 20%, respectively, in both IR spectra of hybrids produced by melt and solution intercalation.

Compared with the clear difference in XRD patterns of hybrids made via two methods, no difference is found in FTIR spectra of the hybrids made via these two methods. Even though the hybrids with low PEO content have different gallery sizes via solution intercalation (4.7–5.3 Å) from those via melt intercalation (8.26 Å),

they do not show significant different vibrations in FTIR spectra. This implies that the conformation of PEO chains in the gallery does not change much with the PEO concentration in the gallery in both melt and solution intercalation. The conformation of PEO chains in more filled galleries (8.3 Å) appear to be similar to that in less filled ones (4.7–5.3 Å).

3.4. Conformation of PEO chains in the hybrids

Some models for the conformation of PEO chains in the gallery of PEO/MMT hybrids have been previously proposed, based on different experimental results. Helical conformation of one-layer PEO was supported by IR and ^{13}C NMR results of hybrids with saturated PEO content in clay gallery [37,38]. A planar zigzag conformation of single or double layers was alternately proposed based on the XRD results on hybrids with various PEO contents [26]. The hybrids in both reports were made via solution intercalation in water or acetonitrile. In contrast to these highly ordered structural models, a random conformation of PEO in the layered silicate galleries has been proposed to address the issues of cation coordination and silicate surface structure [41].

Firstly, from this work, the gallery size of the PEO/MMT hybrid increases with increasing PEO content in solution intercalation. The gallery size shows a gradual increase from 4.7 to 5.3 Å with PEO for low PEO concentrations (less than 15%), rapidly increasing to 8.3 Å, remaining constant for higher PEO contents. The size of PEO chains with a stated helical conformation has been thought to be about 8 Å [37,38]. The gallery size could thus not be much less than this value if PEO took up the conformation of a well-formed, helical shape for all PEO concentrations. The results on the gallery size from XRD data (much less than 8 Å) seems to support the planar zigzag conformation of single or double PEO layers proposed by Wu and Lerner [26]. However, the fact that the gallery size increases gradually from 4.7 to 5.3 Å for low PEO contents cannot be well explained using the proposed conformation of the planar zigzag conformation of single or double PEO layers.

The gallery size of the PEO/MMT hybrids made via melt intercalation appears not to change at all with the PEO content. Even when the PEO content is only 2 wt%, the gallery size of the hybrid is already 8.3 Å. Melt intercalation appears more likely to be one-step process and seems to support the helical, one-layer conformation. It appears from these two earlier experiments that PEO in the same PEO/MMT hybrids might have different conformations because of the different preparative methods.

Secondly, no significant difference has been observed in the FTIR spectra between the hybrids with the same polymer/silicate ratio made via both intercalation methods. The assumption that melt intercalation would create a quite different conformation from solution intercalation appears not to be the case. PEO may have a similar conformation in the hybrid gallery, regardless of the PEO content and the preparation method of the PEO/MMT hybrid. Furthermore, no evidence of the *trans* conformation, an important indicator for the planar zigzag PEO chains, has been observed in all the FTIR spectra of the PEO/MMT system in previously reported research [37,38], nor in these studies of solution and melt intercalation. Rather, the CH_2 rocking vibrations for *gauche* conformation which are important evidence of helical structures, have been observed in both previous reports [37,38] and in this work, although differences appear in the spectra of the current study, compared to previous result. From the IR data, the hypothesis of the presence of zigzag conformations of either single or double PEO layers does not seem likely.

Thirdly, PEO/B34 hybrids exhibit very similar characteristics to PEO/MMT hybrids. They show only one gallery size as a function of PEO content due to melt intercalation and have different gallery sizes as a function of concentration of PEO in the gallery for solution intercalation. PEO shows similar behavior in the galleries of either MMT or B34, which have sodium or organic ammonium cations, and appears to have same conformation in both silicates. Note that the gallery distance is different in both cases.

From the above discussion, a distorted or stretched helical shape may be a better description of the conformation of PEO chains in the gallery of layered silicate. The helical structure of PEO may be readily stretched are distorted, depending on the preparative method. The current FTIR results do not strongly support the presence of a well-formed helical structure. The CH_2 rocking vibrations for the *gauche* configuration either shift or disappear. The implies that a well-formed helical structure is not present, but rather a distorted helical structure is likely in the silicate gallery, especially for low PEO content from solution intercalation.

A proposed schematic structure is thus shown in Fig. 9. The rectangles represent the silicate layers and the circles, the curved lines stand for the organic cations in silicate galleries and ellipses illustrate the PEO chains. Only a single chain is drawn between layers in this figure. The PEO chains are thought to be isolated and remain individually in the gallery between layers along any direction in the *ab* plane. According to this structural proposal, a possible explanation of changes of the gallery size can thus be made. The PEO chains are random coils when dissolved in a solvent and may not be energetically or entropically able to form the 8.3 Å helical conformation when they enter the silicate gallery at low polymer concentration. They form only a distorted helical structure with above 4.7 Å in the *c* direction within the gallery when PEO content is about 2%. As more polymer chains intercalate into the gallery, the chains reduce their dimensions in *ab* plane (in particular a length reduction) to accommodate each other. They, therefore, have to increase the diameter perpendicular to the chain direction (the dimension along the *c* direction in the

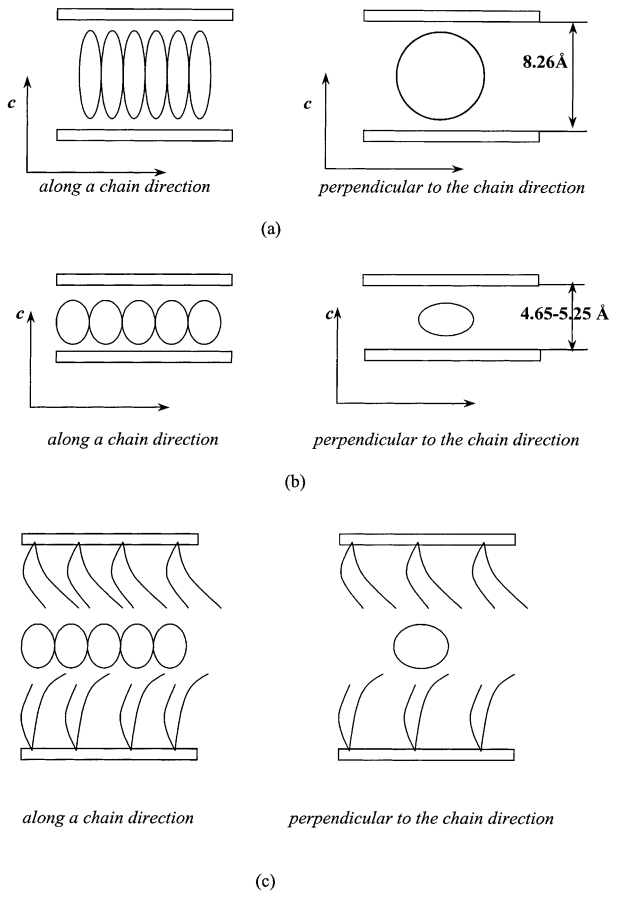

Fig. 9. A proposed schematic structure of a highly distorted helical conformation of PEO chains in the hybrid gallery with (a) smaller gallery size, (b) greater gallery size, and (c) in an organically-modified gallery. The rectangle represents the silicate layer, the circles or ellipses represent PEO chains. The curved lines in (c) represent alkyl ammonium ions

gallery) and this leads to an increase in the gallery size. At low PEO concentration this increase is small, from 4.7 to 5.3 Å. When the PEO content in a particular gallery increases to a possibly critical value, some of the chains from the helical structure and expand the gallery to 8.3 Å. The hybrid contains a distribution of a range of these states for intermediate PEO contents. Such a structural model with a stretched helical conformation of PEO can thus explain the experimental aspects observed in solution intercalation. A comparison can be made with the melt intercalation process. PEO is highly crystalline in bulk PEO and when it is heated into the molten state, although it loses its crystalline characteristics, not all the helical conformation may be lost (albeit becoming distorted). When PEO chains move from the molten bulk into the silicate gallery, they tend to remain or more readily recover their helical structure in which the energy is a minimum. The annealing process may also provide PEO chains the energy for the possible (at least partial) recovery of the helical structure. The energy is sufficient for PEO chain to retain the distorted helical structure in the silicate galleries even for low amounts of PEO. This can also explain the same gallery size in the hybrids with various PEO contents, which is found via melt intercalation.

In addition, the different gallery sizes in the PEO/MMT and PEO/B34 systems can also be explained using this structural model. Since the environment of the confined PEO chains is different in the two systems, the degrees of the distortion of the PEO helical chains could be different. However, more work is needed to confirm the hypothesis, especially, the effect of organic cations on PEO conformation in precisely the same silicate galleries.

4. Conclusion

This paper has compared melt intercalation with solution intercalation using the same PEO/layered silicate systems. XRD and FTIR were used as main techniques to compare the differences and similarities of the final hybrid produced via different preparation methods. The PEO/MMT and PEO/B34 systems with various ratios of PEO/layered silicate have been investigated. A structural model of PEO/layered silicate hybrids, especially of the PEO conformation in the gallery of such hybrids, has been proposed.

The hybrids with various PEO/silicate ratios have shown quite different XRD patterns via two intercalation methods. In solution intercalation, the gallery size deducted from the basal *d*-spacing of hybrid and original MMT increases with the PEO content, from 4.7 to 5.3 Å when PEO is less than 15%. The gallery size reaches 8.3 Å when the PEO content reaches 15% and remains constant for further PEO additions. However, in melt intercalation, the gallery size is always 8.3 Å, even when the PEO content is low, such as for 2% PEO. The previous structural models in the literature propose either a helical structure or a single- and double-layer zigzag conformation, but cannot explain well both results obtained via these methods.

FTIR spectra of the hybrids that contained the same PEO/silicate ratio in the same system but are intercalated via the two different methods do not show any observed difference in terms of the positions of the infrared absorption bands and their relative intensities. The CH_2 rocking vibrations at 950 and 840 cm^{-1} for the *gauche* conformation (an important evidence of helical conformation of PEO) either shift or disappear compared to those in pure, bulk PEO, in which PEO has a helical conformation with a dimension of about 8 Å perpendicular to the chain direction. In addition, the CH_2 rocking vibrations at 1320 cm^{-1} for the *trans* conformation for all samples, evidence of the planar zigzag conformation, are not observed. A highly distorted helical structural is proposed to be a better description of the conformation of PEO chains in the gallery of layered silicates. The helical structure of PEO may be easily distorted (stretched) and recovered in three dimensions like a soft spring. The PEO chain becomes stretched and elongated to enter the silicate gallery when the PEO content is low via solution intercalation, and the gallery size is thus

4.7–5.3 Å. The PEO chains reduce their length to accommodate more PEO chains entering the gallery when PEO content increases. The gallery expands to 8.3 Å for concentration of PEO greater than 15%. Likewise, in melt intercalation, the PEO chains diffuse from molten bulk polymer to the silicate gallery and probably have sufficient energy to maintain their helical structure upon entering.

References

[1] Fukushima Y, Okada A, Kawasumi M, Kurauchi T, Kamigaito O. Clay Miner 1988;23:27.
[2] Okada A, Kawasumi M, Usuki A, Kojima Y, Kurauchi T, Kamigaito O. Mater Res Soc Proc 1990;171:45.
[3] Greenland DG. J Colloid Sci 1963;18:647.
[4] Francis CW. Soil Sci 1973;115:40.
[5] Ruiz-Hitzky E. Adv Mater 1993;5:334.
[6] Lemmon JP, Lerner MM. Chem Mater 1994;6:207.
[7] Tohoh M. European Patent 0479031A1; 1990.
[8] Ogata N, Jimenez G, Kawai H, Ogihara T. J Polym Sci, Part B: Polym Phys 1997;35:389.
[9] Choi HJ, Kim SG, Hyun YH, Jhon MS. Macromol Rapid Commun 2001;22:320.
[10] Chen X, Gonsalves KE. J Mater Res 1997;12:274.
[11] Joen HG, Jung HT, Hudson SD. Polym Bull 1998;42:107.
[12] Kawasumi M, Hasegawa N, Usuki A, Okada A. Mater Engng Sci C 1998;6:135.
[13] Theng BKG. Formation and properties of clay–polymer complexes. New York: Elsevier, 1979.
[14] Vaia RA, Ishii H, Giannelis EP. Chem Mater 1993;5:1694.
[15] Vaia RA, Vasudevan S, Krawiec W, Scanlon LG, Giannelis EP. Adv Mater 1995;7:154.
[16] Krawiec W, Scanlon LG, Fellner JP, Vaia RA, Vasudevan S, Giannelis EP. J Power Sources 1995;54:310.
[17] Vaia RA, Jandt KD, Kramer EJ, Giannelis EP. Macromolecules 1995;28:8080.
[18] Sikka M, Cerini LN, Ghosh SS, Winey KI. J Polym Sci, Part B: Polym Phys 1996;34:1443.
[19] Laus M, Francescangeli O, Sandrolini F. J Mater Res 1997;12:3134.
[20] Liu L, Qi Z, Zhu X. J Appl Polym Sci 1999;71:1133.
[21] Liao B, Song M, Liang H, Pang Y. Polymer 2001;42:10007.
[22] Kojima Y, Usuki A, Kawsumi M, Okada A, Kurauchi T, Kamigaito O, Kaji K. J Polym Sci, Part B: Polym Phys 1994;32:625.
[23] Giannelis EP, Chen H, Demeter J, Manias E, Hadjichristidis N, Karim A. Polym Prepr, Div Polym Chem Am Chem Soc 1999;40:91.
[24] Shen Z, Simon GP, Cheng Y-B. J Aust Ceram Soc 1998;34:1.
[25] Shen Z, Simon GP, Cheng Y-B. Polym Engng Sci 2002, in press.
[26] Wu J, Lerner MM. Chem Mater 1993;5:835.
[27] Davidson WHT. Chem Soc Lond J 1995:3270.
[28] Kuroda Y, Kubo M. J Polym Sci 1957;26:323.
[29] Kuroda Y, Kubo M. J Polym Sci 1959;36:453.
[30] Tadokoro H, Chatani Y, Yoshihara T, Tahara S, Murahashi S. Makromol Chem 1964;73:109.
[31] Matsuura H, Miyazawa T. J Polym Sci A-2 1969;7:1735.
[32] Maxfield J, Shepherd IW. Polymer 1975;16:505.
[33] Koenig JL, Angood AC. J Polym Sci A-2 1970;8:1787.
[34] Liu K-J, Parsons JL. Macromolecules 1969;2:529.
[35] Takahashi Y, Tadokoro H. Macromolecules 1973;6:672.
[36] Papke BL, Ratner MA, Shriver DF. J Phys Chem Solids 1981;42:493.
[37] Ruiz-Hitzky E, Aranda P. Adv Mater 1990;2:545.
[38] Aranda P, Ruiz-Hitzky E. Chem Mater 1992;4:1395.
[39] Aranda P, Ruiz-Hitzky E. Acta Polym 1994;45:59.
[40] van der Marel HW, Beutelspacher H. Atlas of infrared spectroscopy of clay minerals and their admixtures. Amsterdam: Elsevier, 1976. p. 31–58, 113–43.
[41] Bujdak J, Hackett E, Giannelis EP. Chem Mater 2000;12:2168.
[42] Theng BKG. Chemistry of clay–organic reactions. London: Hilger, 1974.
[43] Webb SW, Stanley DA, Scheiner, B. An infared examination of ion-exchanged montmorillonite treated with polyethlene oxide, RI 9036, US Bureau of Mines, 1986.
[44] Hummel DO. Atlas of polymer plastics analysis: Volume1/Band 1, Defined polymers, 3rd ed., Hanser Publishers & VCH Publishers, 1991. p. 258–9, 460–3.
[45] Biasci L, Aglietto M, Ruggeri G, Ciardelli F. Functionalization of montmorillonite by methyl methacrylate polymers containing side-chain ammonium cations. Polymer 1994;35:3296.